

Communication

Electron-Transfer Properties of Phenyleneethynylene Linkers Bound to Gold via a Self-Assembled Monolayer of Molecular Tripod

Toshikazu Kitagawa ^{1,*}, Takashi Kawano ¹, Takahiro Hase ¹, Ikuma Hayakawa ¹, Katsuyuki Hirai ² and Takao Okazaki ¹

- ¹ Department of Chemistry for Materials, Graduate School of Engineering, Mie University, Tsu, Mie 514-8507, Japan; doragonnaito0723@yahoo.co.jp (T.K.); hase@kuroganekasei.co.jp (T.H.); alc2014jp@gmail.com (I.H.); okazaki@chem.mie-u.ac.jp (T.O.)
² Organization for the Promotion of Regional Innovation, Mie University, Tsu, Mie 514-8507, Japan; hirai@chem.mie-u.ac.jp
* Correspondence: kitagawa@chem.mie-u.ac.jp; Tel.: +81-59-231-9416

Received: 23 September 2018; Accepted: 30 October 2018; Published: 6 November 2018



Abstract: The three-point adsorption of tripod-shaped molecules enables the formation of robust self-assembled monolayers (SAMs) on solid surfaces, where the component molecules are fixed in a strictly upright orientation. In the present study, SAMs of a rigid molecular tripod consisting of an adamantane core and three CH₂SH groups were employed to arrange ferrocene on a gold surface through oligo(*p*-phenyleneethynylene) linkers. Cyclic voltammetry of the monolayers demonstrated high surface coverage of ferrocene, yet the molecular interaction among adjacent ferrocene units was negligible. This was because of the extended intermolecular distance caused by the bulky tripod framework. The rates of electron transfer from the ferrocene to the gold surface through different linker lengths were determined by electrochemical measurements, from which the decay factor for oligo(*p*-phenyleneethynylene) wire was evaluated.

Keywords: molecular tripod; self-assembled monolayer; electron transfer; adamantane; ferrocene

1. Introduction

Self-assembled monolayer (SAM) of thiolates on a gold surface, produced by the tight Au–S bonding, creates a secure molecule–metal junction [1–4]. The thermodynamically favored chemisorption of molecules enables monolayer formation simply by forcing thiols to make contact with a clean gold surface. The resultant dense SAMs have been applied to sensors [5,6], molecular machines [7,8], and molecular electronic devices [9–11]. In particular, a SAM of electron-transporting molecules could serve as an excellent junction between the device molecule and a metal electrode.

The component molecules in a densely packed SAM, however, are subjected to severe steric and electrostatic interactions, which can exert an undesirable mutual intermolecular influence that can potentially alter the structural and electronic features of the original molecules in their isolated state. This would hamper the design and utilization of the single-molecule functionalities of the monolayers.

The use of tripod-shaped anchors may be, due to their surface-demanding nature, effective in avoiding such interactions by isolating the molecules within a SAM. A variety of SAMs composed of tripodal trithiols have been reported using the sp³-hybridized carbon [10,12,13] or silicon [14] atom as a central tetrahedral core. Other tripods have utilized the rigid carbon framework of adamantane, in which the four bridgehead bonds extend in the tetrahedral direction [15–21]. A cyclohexane ring, which has a partial structure of adamantane, was also used as a core carbon framework for three thiol legs [22,23]. Previously, we reported a tripod molecule **1** [16–19,21] and its ferrocenyl derivative

2a [18–20], consisting of a rigid adamantane core and three CH_2SH legs (Figure 1). X-ray photoelectron spectroscopy (XPS) studies supported the three-point adsorption of these molecules on the Au(111) surface [20], and a perpendicular orientation of the molecule was shown by DFT optimization [21].

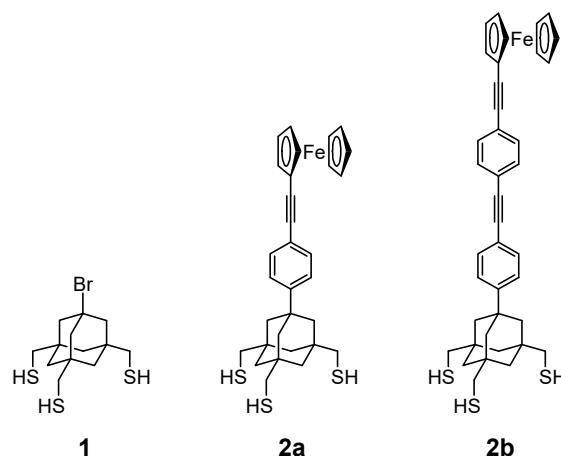


Figure 1. Tripod-shaped trithiols with an adamantane core.

Based on the results of scanning tunneling microscopy (STM) studies, the SAM of **1** is hexagonally arranged with a closest molecular distance of 8.7 Å (Figure 2a) [16]. This distance is significantly larger than that normally observed for the SAMs of linear alkanethiols (5.0 Å) [2,4,24] and allows molecule **2a** to arrange in the same density, wherein neighboring ferrocenyl groups are isolated from each other (Figure 2b) [20]. This feature is highly desirable for the study of the electron transport properties of π -conjugated molecular wires, such as oligo(p -phenyleneethynylene) or $-(\text{C}_6\text{H}_4-\text{C}\equiv\text{C})_n-$. The connection of the straight, rod-like structure of this wire to the adamantane tripod is of particular interest, since the wire may be kept upright in the SAM without intermolecular contact.

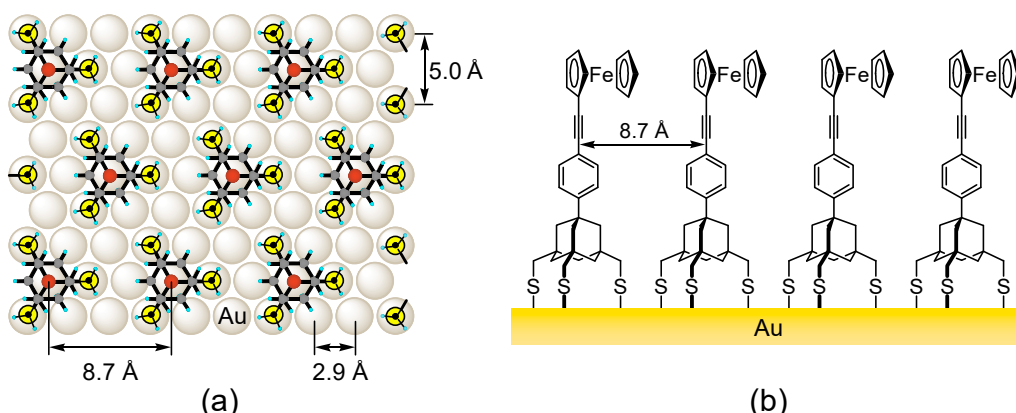


Figure 2. (a) Proposed molecular orientation of the SAMs of **1** on the Au(111) surface; and (b) the schematic diagram of the SAM of ferrocene-terminated trithiol **2a** on a gold surface.

In this paper, we report the electron transfer behavior of p -phenyleneethynylene bridges joining ferrocene and gold substrate using the SAMs of **2a** and **2b** via electrochemical techniques. Reliable single-molecule properties were expected, owing to the independence of each component molecule from neighboring molecules. The decay of the electron transfer rate through the molecule was discussed by comparing the results from the two SAMs.

2. Results and Discussion

2.1. Reductive Desorption

The SAMs were formed by immersing a Au(111) substrate, prepared by vacuum deposition of gold on mica, into a dichloromethane solution of **2a** or **2b** at ambient temperature. Thiol–gold SAMs generally undergo desorption of thiolate ion by electrochemical reduction according to Equation (1) [25–31].



where Au(s) represents the gold atom on the solid surface.

Previously, we reported that the SAMs of **1** and **2a** show a reductive desorption peak in cyclic voltammetry [16,20]. The cyclic voltammetry of the SAM of **2b** at negative potentials in aqueous KOH also showed an irreversible reduction peak at -1.024 V versus Ag/AgCl (Figure 3). The peak potential (E_p), charge density of the reductive wave (Q_{red}), and full width at half-maximum (ΔE_{fwhm}) of related SAMs are summarized in Table 1.

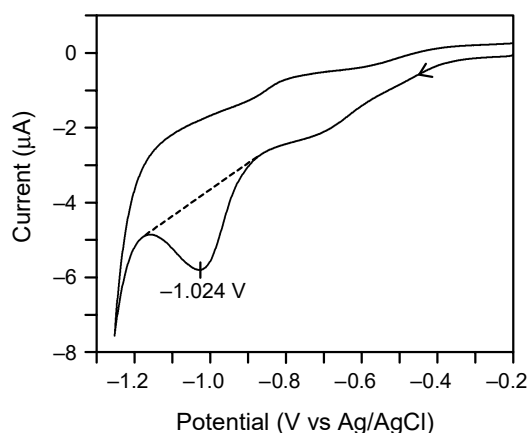


Figure 3. Reductive desorption of the SAM of **2b** on Au(111), as observed by cyclic voltammetry using the surface-modified gold substrate as a working electrode in 0.5 M aqueous KOH. The scan rate was 0.02 V/s. The geometric area of the working electrode was 0.152 cm^2 . The charge for reductive desorption was calculated from the area below the dotted line.

Table 1. Peak potential (E_p), charge density (Q_{red}), and full width at half-maximum (ΔE_{fwhm}) for the electrochemical reductive desorption of SAMs derived from trithiols and dodecanethiol on Au(111). ^a

Thiol	E_p (V vs. Ag/AgCl)	$Q_{\text{red}}^{b,c}$ ($\mu\text{C}/\text{cm}^2$)	ΔE_{fwhm}^c (mV)	Reference
1	−1.088	100	91	[16]
2a	−0.977	91	125	[20]
2b	−1.024	93	134	This work
<i>n</i> -C ₁₂ H ₂₅ SH	−1.084	100	20	[16]

^a Measured by cyclic voltammetry in 0.5 M aqueous KOH. The scan rate was 0.02 V/s. All measurements were performed using the same instrumentation and protocol in the same laboratory to allow comparison. ^b Calculated from the reduction peak area. ^c The uncertainty due to sample-to-sample variations was $\pm 10\%$.

The SAMs of long-chain *n*-alkanethiols, such as *n*-dodecanethiol, are known to show a large negative E_p ($<-1.0\text{ V}$) because the adsorbed molecules resist desorption due to strong attractive interactions between closely neighbored, van der Waals-contacting alkyl groups [30]. Although such interactions are small in the SAMs of tripod molecules **2a** and **2b**, large negative reduction potentials were similarly observed for these molecules. This can be attributed to tighter binding of the molecules to the substrate by the three S–Au bonds.

The small ΔE_{fwhm} for *n*-dodecanethiol can also be ascribed to the strong attractive interaction between neighboring alkyl chains [30], while the much larger values observed for tripod thiols indicate the insignificance of such interactions. The Q_{red} of the SAM of **2b** is comparable to that of **2a**, indicating that, despite the extended molecular length of **2b**, its SAM is as densely packed as in the case of **2a**.

2.2. Oxidation of the Ferrocenyl Group

The cyclic voltammograms of the SAMs of **2a** and **2b** at positive potentials showed reversible redox waves at approximately 0.4 V versus Ag/AgNO₃, owing to the single-electron oxidation of the ferrocenyl group. The redox charges, calculated from the mean value of oxidation and reduction peak areas, were $Q_{\text{ox}} = 24 \pm 2 \mu\text{C}/\text{cm}^2$ for both SAMs. This corresponds to a surface coverage ($\Gamma = Q_{\text{ox}}/F$, where F is the Faraday constant) of $2.5 \times 10^{-10} \text{ mol}/\text{cm}^2$ and indicates that the molecules were packed as densely as in the SAM of **1**. If each of the **2a** and **2b** molecules are adsorbed by three sulfur atoms, the reductive desorption charge is expected to be $3\Gamma = 72 \mu\text{C}/\text{cm}^2$. Considering that approximately 30% of the additional reductive charge is often observed upon desorption of S–Au SAMs due to the change in double layer capacitance, a Q_{red} value of $94 \mu\text{C}/\text{cm}^2$ is expected. The observed values for Q_{red} for the SAM of **2a** and **2b** approximate this value, which supports a secure three-point adsorption.

At sufficiently low scan rates (<0.1 V/s), the full width at half-maximum (ΔE_{fwhm}) and the cathodic to anodic peak separation (ΔE_{pp}) approximated those predicted for an ideal Nernstian redox system ($\Delta E_{\text{fwhm}} = 90.6 \text{ mV}$ and $\Delta E_{\text{pp}} = 0 \text{ mV}$) [32], which indicated that each ferrocenyl group in these SAMs was well isolated from its neighboring molecules. In this scan rate region, ΔE_{pp} was not affected by the scan rate variation.

Upon increasing the scan rate over 0.1 V/s, both SAMs showed a gradual increase in ΔE_{pp} (Figure 4), which is typical of a kinetic outcome involving the rate of electron transfer through adsorbed material. Figure 5 illustrates the plots of the anodic and cathodic peak potentials relative to the formal potential E^0 on the natural logarithm of the scan rate. Based on the increases in ΔE_p as a function of the scan rate, the rate constant of electron transfer (k_{ET}) was estimated using Laviron's Equation (2) [33], resulting in values of 40 ± 5 and $28 \pm 4 \text{ s}^{-1}$ for the SAMs of **2a** and **2b**, respectively.

$$k_{\text{ET}} = \alpha n F v_0 / RT \quad (2)$$

where n is the number of electrons transferred per molecule ($n = 1$ in the present case), F is the Faraday constant, R is the gas constant, and T is the temperature (298 K). v_0 is the scan rate at the intercept of the fit line (dashed lines in Figure 5) with the horizontal line $E_p - E^0 = 0$. The transfer coefficient, α , was set to 0.5.

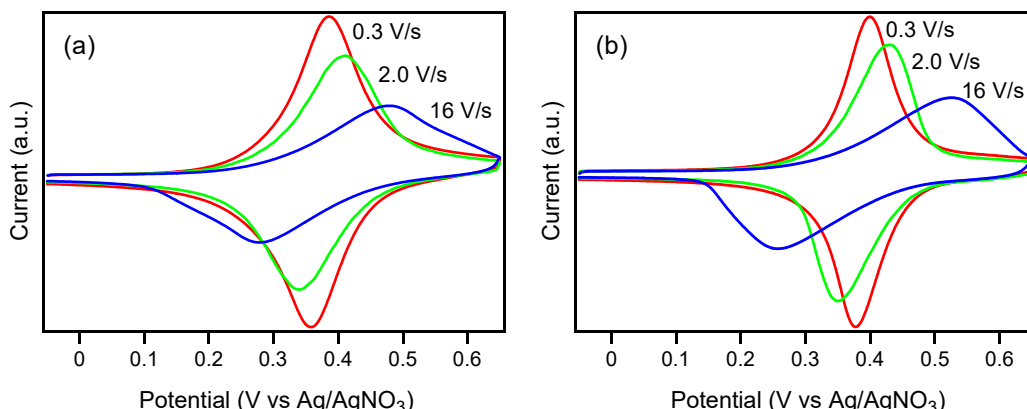


Figure 4. Cyclic voltammograms of the SAM of (a) **2a** and (b) **2b** recorded at different scan rates in CH₂Cl₂ containing 0.1 M TBAP as a supporting electrolyte. The geometric area of the working electrode was 0.152 cm².

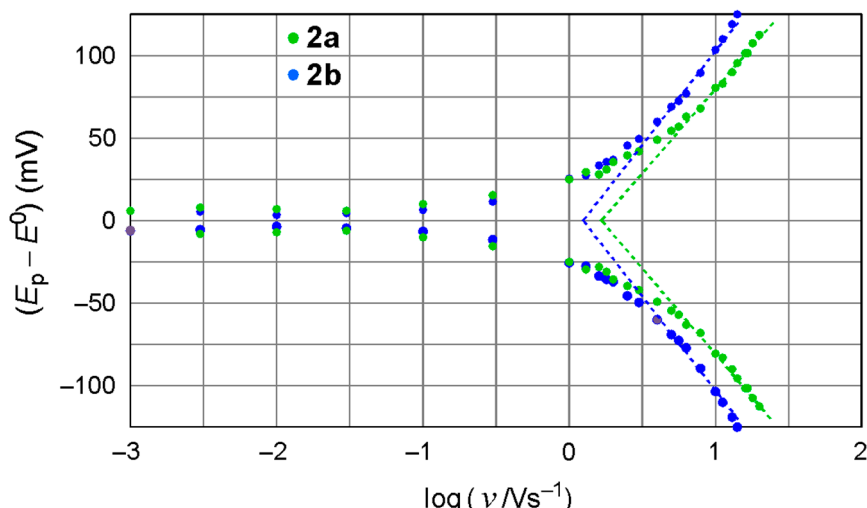


Figure 5. Plot of $E_p - E^0$ versus the logarithm of scan rate for the SAMs of **2a** and **2b** on Au(111). E^0 was 0.371 and 0.392 V versus Ag/Ag⁺ for **2a** and **2b**, respectively.

2.3. Dependence of the Electron Transfer Rate on Distance

In general, the electron transfer rate decays exponentially with distance, as follows.

$$k_{\text{ET}} = k_0 \exp(-\beta r) \quad (3)$$

where k_0 is the preexponential factor and β is the decay constant. The distances (r), taken from the plane determined by the three sulfur atoms to the carbon atom in the ferrocene attached to the ethynyl carbon, were estimated to be 12.9 and 19.7 Å in the SAMs of **2a** and **2b**, respectively, from the DFT optimized structure of the trithiols (Figure 6). On the basis of the deceleration of the electron transfer from 40 s⁻¹ (**2a**) to 28 s⁻¹ (**2b**), the decay constant (β) was derived to be 0.05 Å⁻¹.

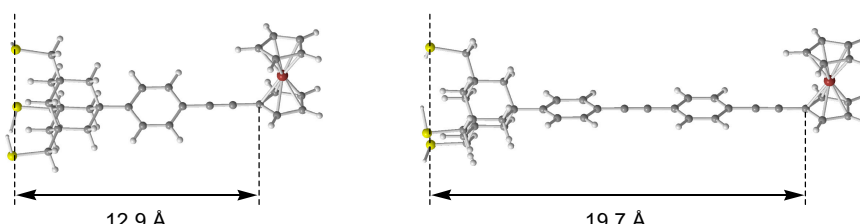


Figure 6. Structures of trithiol **2a** (left) [20] and **2b** (right) optimized at the B3LYP/3-21G(d)-LANL2DZ level.

The β values for similar, but adamantane-free, oligo(*p*-phenyleneethynylene) wires substituted with methyl and propoxy groups were reported by Creager et al. ($\beta = 0.36 \text{ \AA}^{-1}$, $n = 3-6$) [34] and by Sachs et al. ($\beta = 0.57 \text{ \AA}^{-1}$, $n = 2, 3$) [35] using non-electroactive diluent thiols. The $r-\ln k_{\text{ET}}$ plot in Figure 7 shows their data, together with our results and those reported by Creager for linear alkyl chain wires, $\text{FcCONH(CH}_2\text{)}_m\text{S-Au(s)}$ ($m = 7-10$ and 15) [36].

A significant feature of our data is the extremely slow electron transfer, by a factor of approximately e^{-10} ($<10^{-4}$), compared with that reported for adamantane-free oligo(*p*-phenyleneethynylene) wires. The reason could be the insertion of an aliphatic adamantyl group into our molecule. Another important point is that although all lines in Figure 7, except for that of the present work, converge to $\ln k_{\text{ET}} = 23$ at $r = 0$, which corresponds to the common limit at zero distance, our data extrapolates to a much lower value, $\ln k_{\text{ET}} \sim 4$. This could also be caused by the presence of the adamantane tripod acting as a resistor between the end of the conjugated wire and the gold.

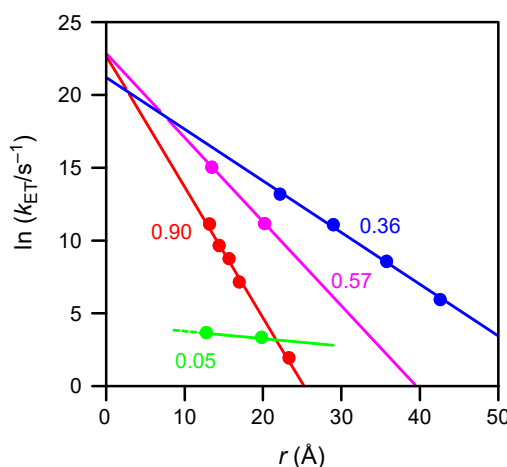


Figure 7. Plots of $\ln k_{ET}$ versus distance for SAMs of molecular wires bridging ferrocene and gold via S–Au bonding. Green (this work), blue [34], and purple [35]: oligo(*p*-phenyleneethynylene) wire. Red [36]: linear alkylamide wire. Values of β are indicated.

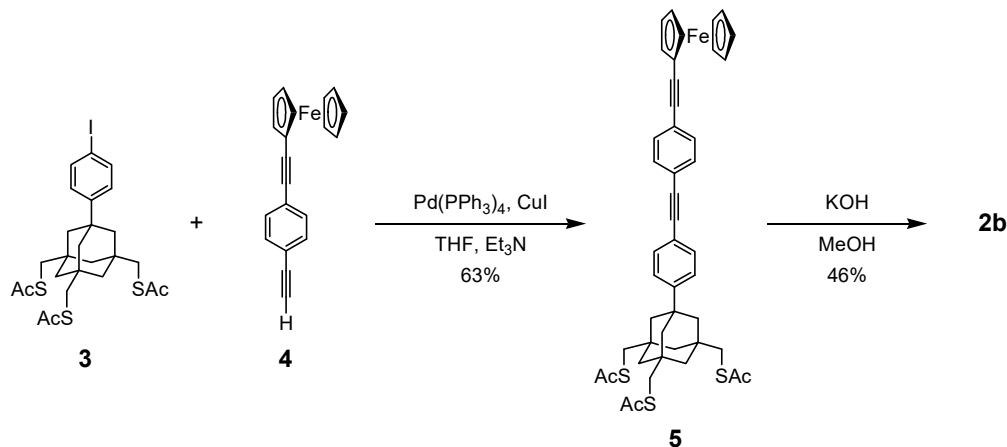
The cause of the very small β (0.05 \AA^{-1}) of our linker is unclear. A possible cause of the large difference between this value and other oligo(*p*-phenyleneethynylene) wires in Figure 7 could be the electrolyte used for our measurement (TBAP in CH_2Cl_2), which has a lower polarity than either aqueous HClO_4 or NaClO_4 that was used in other studies [34,35].

3. Materials and Methods

3.1. Materials

For electrochemical experiments, water was purified using a Millipore Simplicity 185 Water System ($18 \text{ M}\Omega \text{ cm}$ resistivity). Other solvents for electrolyte preparation and the rinsing of glassware were of the highest purity commercially available and were used without further purification. Gold (99.99%) was obtained as a 0.8-mm wire. Mica was purchased from Nilaco (Tokyo, Japan) in the form of a 0.40–0.45-mm natural sheet.

Trithiol **2a** was prepared by the method we reported earlier [20]. Compound **2b** was synthesized by Sonogashira coupling reaction of iodopheny-terminated trithioacetate **3** [16,20] and ferrocene derivative **4** [37] to give **5**, followed by the methanolysis of the three AcS groups (Scheme 1). Details of the synthetic procedure are provided in the Supplementary Materials.



Scheme 1. Synthetic route to elongated trithiol **2b**.

3.2. Preparation of Self-Assembled Monolayers on Gold

Gold substrates with a (111) surface were prepared via vacuum vapor deposition of gold (99.99%) onto freshly cleaved mica sheets (0.05 mm thickness, 6 × 6 cm) under high vacuum ($<10^{-3}$ Pa) at a substrate temperature of 580 °C. The deposition was performed at an evaporation rate of 1.0–1.5 nm/s until a gold thickness of 200 nm was reached. The obtained substrate was cut into 1 × 2 cm pieces and annealed at 530 °C in a furnace for 8 h under air to remove the surface contamination and to minimize defects. SAMs were formed by soaking the substrate in a 0.1 mM solution of trithiols in CH₂Cl₂ for at least 24 h.

3.3. Electrochemical Measurements

Glassware (cells and pipettes, etc.) used for electrochemical measurements were soaked in 10% potassium hydroxide in 2-propanol for 24 h to remove surface organic contaminants, washed thoroughly with deionized water, and dried under air at 100 °C before use. The surface-modified gold substrate was mounted at the bottom of a cone-shaped cell using an O-ring to serve as a working electrode. The area of the electrode exposed to the electrolyte was 0.152 cm² (i.e., a 4.4 mm diameter circle). Reductive desorption was recorded with aqueous 0.5 M KOH using an Ag/AgCl/sat. KCl reference electrode (Supplementary Materials, Figure S5a). Redox waves of a ferrocenyl group were observed using a CH₂Cl₂ solution containing 0.1 M tetrabutylammonium perchlorate (TBAP) and an Ag/AgNO₃ (0.01 M in CH₃CN) reference electrode (Supplementary Materials Figure S5b). The electrolyte solution in the cell was de-aerated by bubbling argon for 10 min before scanning. Voltammograms were recorded using a ALS600C electrochemical analyzer (BAS, Tokyo, Japan).

3.4. Theoretical Calculations

Results of DFT calculations [38] for **2a** were reported earlier [20]. Calculations for **2b** were performed in a similar manner using the Gaussian 03 program [39]. Geometry optimization was carried out using the B3LYP method and general basis set (Gen keyword). The C, H, and S atoms were calculated with the 3-21G(d) basis set, whereas Fe was calculated with the LANL2DZ (5D, 7F) basis set. The results of optimization are shown in Supplementary Materials, Table S1. The obtained geometry was verified by frequency calculations to have no imaginary frequencies.

4. Conclusions

Tripod-shaped trithiols, **2a** and **2b**, bearing a ferrocenyl group via mono and bis(*p*-phenyleneethynylene) linker formed SAMs on Au(111) surface that featured negligible interactions among neighboring ferrocenyl groups, regardless of the high coverage. These SAMs showed k_{ETS} [$40 \pm 5 \text{ s}^{-1}$ (**2a**) and $28 \pm 4 \text{ s}^{-1}$ (**2b**)] that are more than four orders of magnitude smaller than the values reported for linkers of the same type and length. A very small decay constant, $\beta = 0.05 \text{ \AA}^{-1}$, was also observed. These findings can be explained by the fact that a saturated framework of adamantane insulates conjugated *p*-phenyleneethynylene wire and gold. Another possible reason is the low polarity of the electrolyte we employed, compared with those used in other works. Studies on the electron transfer properties of further elongated oligo(*p*-phenyleneethynylene) linkers are in progress. Also, it would be valuable to elucidate the nature of the “resistance” posed by the adamantane framework by the use of directly linked ferrocene–adamantane tripod.

Supplementary Materials: Supplementary materials including synthetic procedures, figures of NMR spectra and cyclic voltammetry cells, and the results of DFT calculations are available online.

Author Contributions: T.K. (Toshikazu Kitagawa) conceived and designed the experiments. T.K. (Takashi Kawano), T.H., and I.H. conducted the experiments. T.K. (Toshikazu Kitagawa) and K.H. analyzed the data. T.O. performed theoretical calculations. T.K. (Toshikazu Kitagawa) wrote the paper.

Funding: This research was funded by MEXT KAKENHI Grant Number JP20027006 and JSPS KAKENHI Grant Number JP15K05474. We also thank the Izumi Science and Technology Foundation for supporting our study.

Conflicts of Interest: The authors declare no conflict of interest.

References

- Ulman, A. Formation and Structure of Self-Assembled Monolayers. *Chem. Rev.* **1996**, *96*, 1533–1554. [[CrossRef](#)] [[PubMed](#)]
- Poirier, G.E. Characterization of Organosulfur Molecular Monolayers on Au(111) using Scanning Tunneling Microscopy. *Chem. Rev.* **1997**, *97*, 1117–1127. [[CrossRef](#)] [[PubMed](#)]
- Love, J.C.; Estroff, L.A.; Kriebel, J.K.; Nuzzo, R.G.; Whitesides, G.M. Self-Assembled Monolayers of Thiolates on Metals as a Form of Nanotechnology. *Chem. Rev.* **2005**, *105*, 1103–1169. [[CrossRef](#)] [[PubMed](#)]
- Kind, M.; Wöll, C. Organic surfaces exposed by self-assembled organothiol monolayers: Preparation, characterization, and application. *Prog. Surf. Sci.* **2009**, *84*, 230–278. [[CrossRef](#)]
- Gooding, J.J.; Mearns, F.; Yang, W.; Liu, J. Self-Assembled Monolayers into the 21st Century: Recent Advances and Applications. *Electroanalysis* **2003**, *15*, 81–96. [[CrossRef](#)]
- Bertin, P.A.; Ahrens, M.J.; Bhavsar, K.; Georganopoulos, D.; Wunder, M.; Blackburn, G.F.; Meade, T.J. Ferrocene and Maleimide-Functionalized Disulfide Scaffolds for Self-Assembled Monolayers on Gold. *Org. Lett.* **2010**, *12*, 3372–3375. [[CrossRef](#)] [[PubMed](#)]
- Van Delden, R.A.; ter Wiel, M.K.J.; Pollard, M.M.; Vicario, J.; Koumura, N.; Feringa, B.L. Unidirectional molecular motor on a gold surface. *Nature* **2005**, *437*, 1337–1340. [[CrossRef](#)] [[PubMed](#)]
- Kay, E.R.; Leigh, D.A.; Zerbetto, F. Synthetic Molecular Motors and Mechanical Machines. *Angew. Chem. Int. Ed.* **2007**, *46*, 72–191. [[CrossRef](#)] [[PubMed](#)]
- Tour, J.M. Molecular Electronics. Synthesis and Testing of Components. *Acc. Chem. Res.* **2000**, *33*, 791–804. [[CrossRef](#)] [[PubMed](#)]
- Hirayama, D.; Takimiya, K.; Aso, Y.; Otsubo, T.; Hasobe, T.; Yamada, H.; Imahori, H.; Fukuzumi, S.; Sakata, Y. Large Photocurrent Generation of Gold Electrodes Modified with [60]Fullerene-Linked Oligothiophenes Bearing a Tripodal Rigid Anchor. *J. Am. Chem. Soc.* **2002**, *124*, 532–533. [[CrossRef](#)] [[PubMed](#)]
- McCreery, R.L. Molecular Electronic Junctions. *Chem. Mater.* **2004**, *16*, 4477–4496. [[CrossRef](#)]
- Fox, M.A.; Whitesell, J.K.; McKerrow, A.J. Fluorescence and Redox Activity of Probes Anchored through an Aminothiol to Polycrystalline Gold. *Langmuir* **1998**, *14*, 816–820. [[CrossRef](#)]
- Wei, L.; Tiznado, H.; Liu, G.; Padmaja, K.; Lindsey, J.S.; Zaera, F.; Bocian, D.F. Adsorption Characteristics of Tripodal Thiol-Functionalized Porphyrins on Gold. *J. Phys. Chem. B* **2005**, *109*, 23963–23971. [[CrossRef](#)] [[PubMed](#)]
- Yam, C.M.; Cho, J.; Cai, C. Preparation, Characterization, and Heck Reaction of Multidentate Thiolate Films on Gold Surfaces. *Langmuir* **2003**, *19*, 6862. [[CrossRef](#)]
- Kittredge, K.W.; Minton, M.A.; Fox, M.A.; Whitesell, J.K. α -Helical polypeptide films grown from sulfide or thiol linkers on gold surfaces. *Helv. Chim. Acta* **2002**, *85*, 788–798. [[CrossRef](#)]
- Kitagawa, T.; Idomoto, Y.; Matsubara, H.; Hobara, D.; Kakiuchi, T.; Okazaki, T.; Komatsu, K. Rigid molecular tripod with an adamantane framework and thiol legs. synthesis and observation of an ordered monolayer on Au(111). *J. Org. Chem.* **2006**, *71*, 1362–1369. [[CrossRef](#)] [[PubMed](#)]
- Katano, S.; Kim, Y.; Matsubara, H.; Kitagawa, T.; Kawai, M. Hierarchical chiral framework based on a rigid adamantane tripod on Au(111). *J. Am. Chem. Soc.* **2007**, *129*, 2511–2515. [[CrossRef](#)] [[PubMed](#)]
- Katano, S.; Kim, Y.; Kitagawa, T.; Kawai, M. Self-assembly and scanning tunneling microscopy tip-induced motion of ferrocene adamantane trithiolate adsorbed on Au(111). *Jpn. J. Appl. Phys.* **2008**, *47*, 6156–6159. [[CrossRef](#)]
- Katano, S.; Kim, Y.; Kitagawa, T.; Kawai, M. Tailoring electronic states of a single molecule using adamantane-based molecular tripods. *Phys. Chem. Chem. Phys.* **2013**, *15*, 14229–14233. [[CrossRef](#)] [[PubMed](#)]
- Kitagawa, T.; Matsubara, H.; Komatsu, K.; Hirai, K.; Okazaki, T.; Hase, T. Ideal redox behavior of the high-density self-assembled monolayer of a molecular tripod on a Au(111) surface with a terminal ferrocene group. *Langmuir* **2013**, *29*, 4275–4282. [[CrossRef](#)] [[PubMed](#)]
- Kitagawa, T.; Nakanishi, S.; Mizuno, A.; Niwa, Y.; Tabata, H.; Hirai, K.; Okazaki, T. Tuning the coverage of self-assembled monolayer by introducing bulky substituents onto rigid adamantane tripod. *ARKIVOC* **2018**, *2*, 131–144. [[CrossRef](#)]

22. Singhana, B.; Rittikulsittichai, S.; Lee, T.R. Tridentate adsorbates with cyclohexyl headgroups assembled on gold. *Langmuir* **2013**, *29*, 561–569. [CrossRef] [PubMed]
23. Singhana, B.; Jamison, A.C.; Hoang, J.; Lee, T.R. Self-assembled monolayer films derived from tridentate cyclohexyl adsorbates with alkyl tailgroups of increasing chain length. *Langmuir* **2013**, *29*, 14108–14116. [CrossRef] [PubMed]
24. Kakiuchi, T.; Iida, M.; Gon, N.; Hobara, D.; Imabayashi, S.; Niki, K. Miscibility of adsorbed 1-undecanethiol and 11-mercaptopoundecanoic acid species in binary self-assembled monolayers on Au(111). *Langmuir* **2001**, *17*, 1599–1603. [CrossRef]
25. Walczak, M.M.; Popenoe, D.D.; Deinhammer, R.S.; Lamp, B.D.; Chung, C.; Porter, M.D. Reductive desorption of alkanethiolate monolayers at gold: A measure of surface coverage. *Langmuir* **1991**, *7*, 2687–2693. [CrossRef]
26. Widrig, C.A.; Chung, C.; Porter, M.D. The electrochemical desorption of n-alkanethiol monolayers from polycrystalline Au and Ag electrodes. *J. Electroanal. Chem.* **1991**, *310*, 335–359. [CrossRef]
27. Yang, D.-F.; Wilde, C.P.; Morin, M. Studies of the electrochemical removal and efficient re-formation of a monolayer of hexadecanethiol self-assembled at an Au(111) single crystal in aqueous solutions. *Langmuir* **1997**, *13*, 243–249. [CrossRef]
28. Imabayashi, S.; Iida, M.; Hobara, D.; Feng, Z.Q.; Niki, K.; Kakiuchi, T. Reductive desorption of carboxylic-acid-terminated alkanethiol monolayers from Au(111) surfaces. *J. Electroanal. Chem.* **1997**, *428*, 33–38. [CrossRef]
29. Hobara, D.; Miyake, K.; Imabayashi, S.; Niki, K.; Kakiuchi, T. In-situ scanning tunneling microscopy imaging of the reductive desorption process of alkanethiols on Au(111). *Langmuir* **1998**, *14*, 3590–3596. [CrossRef]
30. Kakiuchi, T.; Usui, H.; Hobara, D.; Yamamoto, M. Voltammetric properties of the reductive desorption of alkanethiol self-assembled monolayers from a metal surface. *Langmuir* **2002**, *18*, 5231–5238. [CrossRef]
31. Eggers, P.K.; Zareie, H.M.; Paddon-Row, M.N.; Gooding, J.J. Structure and properties of redox active self-assembled monolayers formed from norbornylogous bridges. *Langmuir* **2009**, *25*, 11090–11096. [CrossRef] [PubMed]
32. Bard, A.J.; Faulkner, L.R. *Electrochemical Methods: Fundamentals and Applications*, 2nd ed.; John Wiley and Sons: New York, NY, USA, 2000; pp. 590–593.
33. Laviron, E. General expression of the linear potential sweep voltammogram in the case of diffusionless electrochemical systems. *J. Electroanal. Chem.* **1979**, *101*, 19–28. [CrossRef]
34. Creager, S.; Yu, C.J.; Bamdad, C.; O'Connor, S.; MacLean, T.; Lam, E.; Chong, Y.; Olsen, G.T.; Luo, J.; Gozin, M.; et al. Electron transfer at electrodes through conjugated “molecular wire” bridges. *J. Am. Chem. Soc.* **1999**, *121*, 1059–1064. [CrossRef]
35. Sachs, S.B.; Dudek, S.P.; Hsung, R.P.; Sita, L.R.; Smalley, J.F.; Newton, M.D.; Feldberg, S.W.; Chidsey, C.E.D. Rates of interfacial electron transfer through π -conjugated spacers. *J. Am. Chem. Soc.* **1997**, *119*, 10563–10564. [CrossRef]
36. Weber, K.; Hockett, L.; Creager, S. Long-range electronic coupling between ferrocene and gold in alkanethiolate-based monolayers on electrodes. *J. Phys. Chem. B* **1997**, *101*, 8286–8291. [CrossRef]
37. Hsung, R.P.; Chidsey, C.E.D.; Sita, L.R. Synthesis and characterization of unsymmetric ferrocene-terminated phenylethynyl oligomers $Cp_2Fe-[C\equiv C-C_6H_4]_n-X$ ($X = SH, SMe, SOMe$, and SO_2Me). *Organometallics* **1995**, *14*, 4808–4815. [CrossRef]
38. Koch, W.; Holthausen, M.C. *A Chemist's Guide to Density Functional Theory*, 2nd ed.; Wiley–VCH: Weinheim, Germany, 2000; ISBN 3-527-30372-3.
39. Frisch, M.J.; Trucks, G.W.; Schlegel, H.B.; Scuseria, G.E.; Robb, M.A.; Cheeseman, J.R.; Montgomery, J.A., Jr.; Vreven, T.; Kudin, K.N.; Burant, J.C.; et al. *Gaussian 03*; Revision E.01; Gaussian, Inc.: Wallingford, CT, USA, 2004.

Sample Availability: Samples of the compounds are available from the authors.



© 2018 by the authors. Licensee MDPI, Basel, Switzerland. This article is an open access article distributed under the terms and conditions of the Creative Commons Attribution (CC BY) license (<http://creativecommons.org/licenses/by/4.0/>).